Broadband laboratory measurements of dispersion in thermally cracked and fluid-saturated quartzite and a synthetic analogue

Yang Li, Melissa Olin, Emmanuel C. David, and Ian Jackson, Australian National University, Canberra
Heather Schijns and Douglas R. Schmitt, University of Alberta, Edmonton

Abstract

In the field, the seismic waves used for active-source imaging typically contain frequencies from 10 to about 100 Hz, with corresponding wavelengths of tens of meters. This contrasts greatly with the ultrasonic (~ 1-MHz) wave-speed measurements carried out in the laboratory, with millimeter wavelengths. The purpose of the laboratory measurements is, of course, to provide insight into seismic wave speeds in situ. However, with the presence of a pore fluid, velocity measurements are sensitive to the frequency at which velocity data are collected. A study focuses on such fluid-flow-related dispersion by performing a broadband measurement in the laboratory from millihertz (mHz) to megahertz (MHz) frequencies on a natural quartzite and on a synthetic sintered glass-bead sample. Thermal cracks that have small aspect ratios of about 10^{-4} to 10^{-3} were introduced in both samples, which are of low porosities (1% to 2%) even after thermal cracking. A seismic-frequency forced-oscillation method is combined with a high-frequency ultrasonic technique, providing access to a wide frequency range. Under water-saturated conditions, the observed seismic wave speeds display substantial variations between seismic and ultrasonic frequencies in the cracked quartzite. A systematic increase in shear modulus, attributed to the suppression of fluid flow, has been monitored on the cracked glass-bead specimen with both argon and water saturation at ultrasonic frequency.

Introduction

Seismic and sonic-logging techniques commonly are used in subsurface exploration for conventional and renewable energy and minerals and are mandated in the monitoring of sequestered carbon dioxide. Seismic-exploration data usually are collected at frequencies ranging from 10 and 100 Hz and from sonic logs at kilohertz (kHz) frequencies. In contrast, laboratory methods traditionally have measured velocities by ultrasonic techniques at megahertz (MHz) frequencies. Therefore, any dependence of seismic wave velocity with frequency, referred to as *dispersion*, adds uncertainties in seismic data interpretation, and this needs to be quantified further by theoretical models and experiments.

The passage of a seismic wave through a fluid-saturated medium creates gradients in pore pressure between cracks of different orientation and between cracks and pores. Conditions are described as "saturated isobaric" if fluid can flow between adjacent cracks or pores to achieve uniform pore pressure within the specimen but without fluid exchange between the pore space of the specimen and an external fluid reservoir. At sufficiently high frequency, such gradients in pore pressure cannot be relaxed by fluid flow between adjacent cracks and pores on the timescale of the wave — conditions that define the saturated-isolated regime. Suppression of such "squirt" or "local" flow results in an increase of the effective elastic moduli, i.e., stiffening of the fluid-saturated medium (O'Connell and Budiansky, 1977; Mavko and Nur, 1975). A broadband measurement of modulus on the same specimen from subhertz to megahertz has the potential to resolve this kind of dispersion (Adam et al., 2009; Batzle et al., 2006).

The theoretical literature on this topic is large, but because controlled experimental tests are rare, the theoretical models still have not been tested thoroughly and unambiguously. Ultrasonic methods have been used for more than 50 years, and the technique is mature. Conversely, progress in the broadband tests was hindered because of the challenging difficulties of making measurements at low frequencies and small strains. Collaborative work combining the seismic-frequency technique at the Australian National University with the capability of low-strain shear-deformation experiments under pressures as high as 300 MPa and the ultrasonic technique at the University of Alberta provides access to velocity data measured over a wide frequency range from subhertz to megahertz.

Previous attempts at broadband measurements have been focused mainly on natural geologic materials such as Fontainebleau Sandstones (David et al., 2013) or carbonates (Adam et al., 2006), the mineralogic complexity of which could complicate the demonstration and interpretation of dispersion related to fluid flow.

This article aims to quantify dispersion associated with fluid flow in media of low porosity and simple crack microstructures by reporting preliminary results from new broadband measurements. We first provide a preview of our new experimental shear-modulus/velocity measurements on a natural quartzite and on a synthetic glass-bead specimen with controlled microstructure. We then examine theoretically the pressure dependence of the observations on cracked quartzite.

Materials and experimental methods

The quartzite specimen, from Cape Sorell, Tasmania, Australia, is dominated by quartz grains about 0.5 mm in diameter. The specimen is translucent light gray with more than 99% quartz by volume and less than 1% muscovite at grain boundaries. Initial porosity is ~ 0.3% for the Cape Sorell quartzite before thermal cracking.

The synthetic analogues were made by sintering soda-lime-silica glass beads (Bouzidi and Schmitt, 2009). First the commercial glass beads were sieved to reach a diameter of approximately 300 μm and were loaded into a cylindrical glass mold. The beads were then sintered at 700°C for 18 hours to result in residual (equant) porosity of about 2%. The newly sintered glass-bead specimen was then precision-ground to a cylindrical shape 50 mm long and 15 mm in diameter.

Because the initial crack porosity for the Cape Sorell quartzite was small and the sintered specimen was almost free of cracks, more cracks needed to be introduced artificially, first to simply allow fluid saturation and to enhance any possible fluid-flow-related dispersion for measurement.

Thermal cracking was performed on both types of samples. The Cape Sorell quartzite was heated to 1100°C and then quenched into liquid nitrogen to increase its porosity to about 2.3%, as measured by mercury-injection porosimetry (Figure 1a). Cracking in this case was likely produced by a combination of thermal shock and the volume changes of the quartz crystals at the α-quartz to β-quartz phase transition at 573°C. The sintered glass-bead specimen was heated to 500°C for two hours and then quenched into liquid water at room temperature to develop thermal-crack networks (Figure 1b) with relatively uniform low crack aspect ratio of about 7×10^{-4} (estimated by scanning electron microscopy [SEM]) and 0.2% crack porosity measured by the dimensional increase caused by thermal cracking. The permeabilities of quartzite and glass-bead specimens after thermal cracking, measured by the pore-fluid equilibrium method (technical details can be found in Schijns [2014]), vary systematically with differential pressure (confining pressure minus pore pressure) between 8×10^{-21} to 5×10^{-20} and 8×10^{-20} to 7×10^{-19} m^2, respectively.

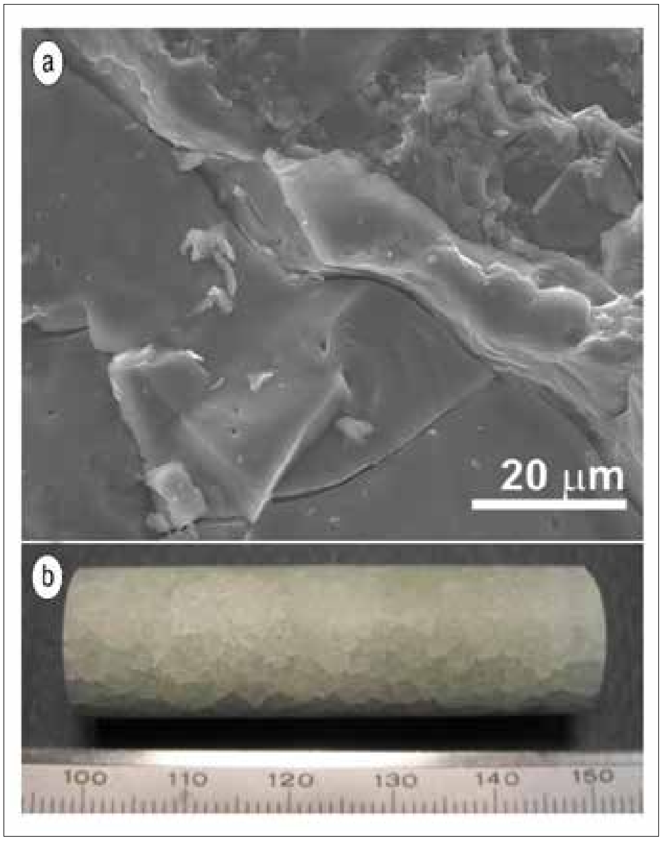

Figure 1. (a) SEM image of the Cape Sorell quartzite after thermal cracking. (b) Thermal cracks introduced into a precision-ground glass-bead specimen by quenching the heated specimen from 500°C into room-temperature liquid water.

For both the Cape Sorell quartzite and the glass-bead specimen, shear modulus was measured at seismic frequencies (millihertz through hertz) with a forced-oscillation method, and shear velocities were measured at ultrasonic frequencies (megahertz) with the ultrasonic-pulse transmission technique. The latter well-established method involves measurement of the traveltime of an ultrasonic pulse generated by a piezoelectric transducer at 1 MHz that travels through the studied sample and finally is received by another piezoelectric transducer at the other end of the sample (Schijns, 2014).

The forced-oscillation method for use at seismic frequencies (Jackson and Paterson, 1993) might be less familiar and therefore is described briefly here. The cylindrical specimen is connected mechanically with a steel elastic standard under pressure to form an integral beam with its top fixed. A seismic-frequency oscillating torque is applied by a pair of electromagnetic drivers near the lower end of the beam. Displacements associated with the twist of the specimen and of the elastic standard are measured by two pairs of

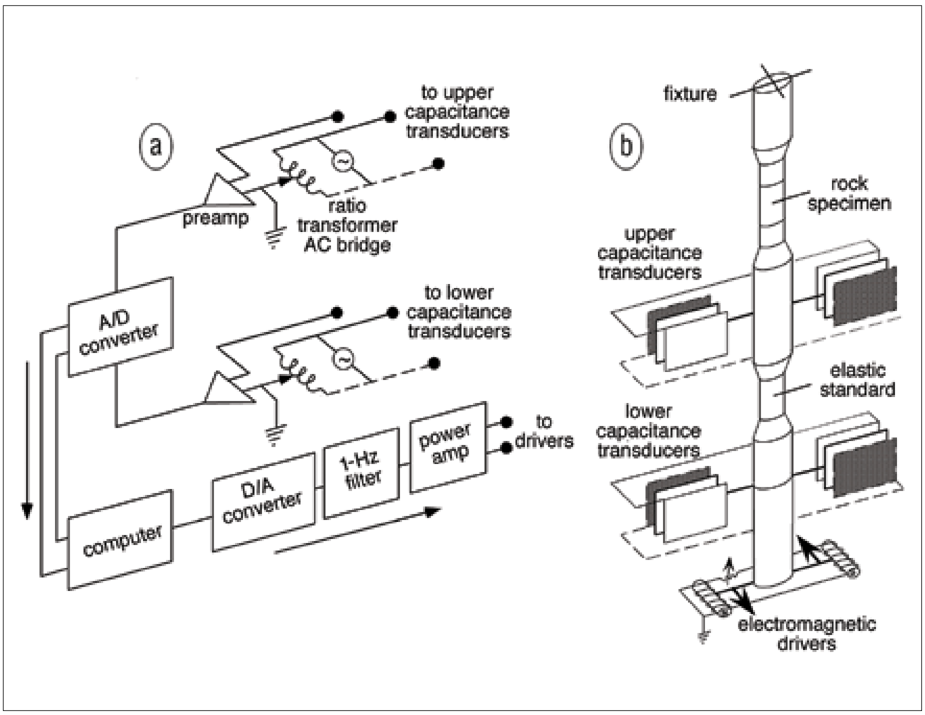

Figure 2. (a) Computer-control and data-acquisition system of the apparatus used for low-frequency forced-oscillation measurements and (b) torsional-mode experimental arrangements with a pair of electromagnetic drivers functioning at the lower end of the cantilevered specimen — elastic standard beam and two pairs of diagonally connected three-plate capacitance transducers.

three-plate capacitance transducers with a precision of measured strain amplitude down to 10^{-8} (Figure 2).

By conducting a parallel experiment with a purely elastic control specimen with the same geometry and known properties under the same conditions, the shear modulus of the studied specimen can be inferred by comparing the behaviors of both. In addition, the phase difference between the studied specimen and the mechanically coupled elastic standard subject to the same oscillation torque can provide information on dissipation ($1/Q$).

The confining pressure was provided by either compressed argon gas on low-frequency attenuation apparatus or hydraulic oil for ultrasonic measurements. Both the Cape Sorell quartzite and the glass-bead specimen were measured under dry, argon-saturated, and water-saturated conditions in sequence, under various conditions of independently controlled confining and pore-fluid pressures. The viscosities of argon (~ 10^{-5} Pa · s) and of water (~ 10^{-3} Pa · s) are different by two orders of magnitude, the contrast of which can significantly change the timescale for fluid equilibrium and shift the characteristic frequencies that separate different fluid-flow regimes.

Specimens were encapsulated in either an annealed copper jacket (for forced-oscillation measurements) or rubber tubing (for ultrasonic measurements) to separate the pore-fluid pressure system from the confining pressure system. In seismic-frequency measurements for the Cape Sorell quartzite, maximum confining and pore pressures were 190 MPa and 140 MPa, respectively. In ultrasonic velocity measurements, confining and pore pressures were limited to 160 MPa and 140 MPa, respectively, for the Cape Sorell quartzite and 100 MPa and 40 MPa, respectively, for the glass-bead specimen.

A systematically varying differential pressure with intervals of about 10 MPa was achieved by setting different combinations of confining and pore pressures. At a targeted differential-pressure level, after waiting adequate time for thermal relaxation and pore-fluid equilibration after each adjustment of pressure, the response of the studied specimen to applied torques was measured at seven oscillation frequencies (10, 21, 46, 87, 156, 260, and 781 mHz) on the attenuation apparatus, and the traveltime of the 1-MHz shear-mode pulse was measured with the ultrasonic-pulse transmission technique.

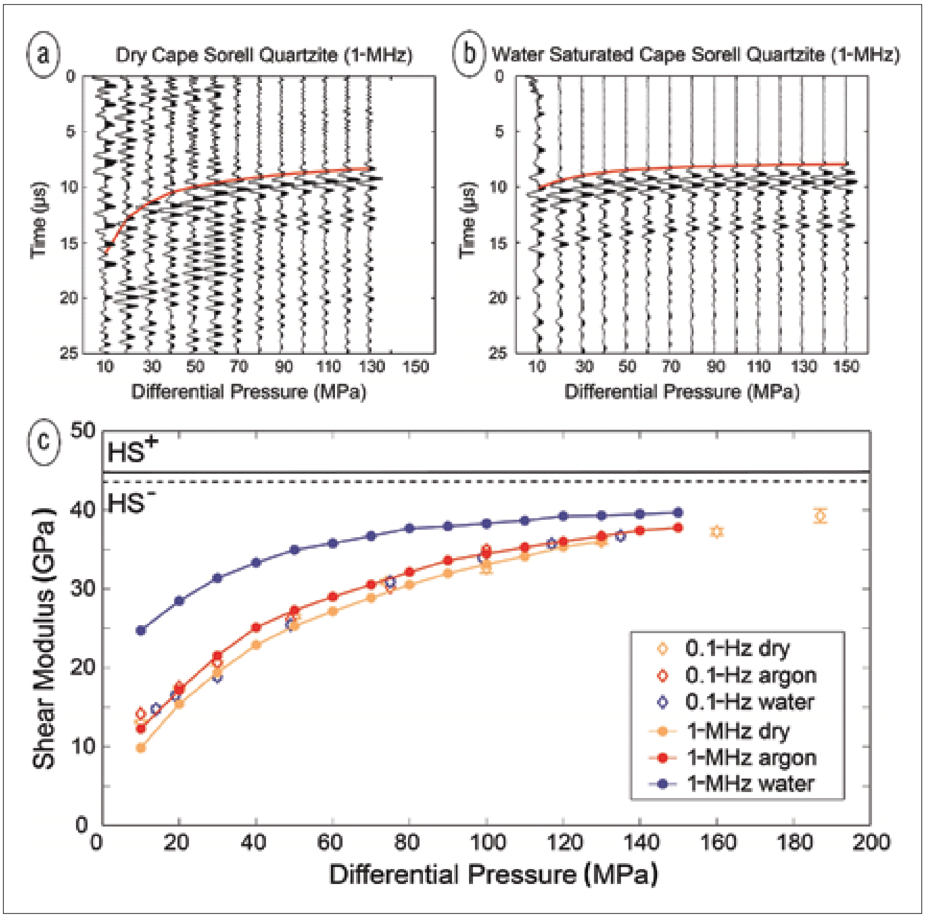

Figure 3. Ultrasonic (1-MHz) shear-wave records, (a) dry and (b) water saturated, for thermally cracked Cape Sorell quartzite. (c) Shear moduli measured at 0.1 Hz and 1 MHz plotted as a function of differential pressure. The Hashin-Shtrikman upper (HS+) and lower (HS–) bounds provide estimates of the expected shear modulus for full dense polycrystalline quartz. The marked effect of crack closure can be observed under dry conditions but is substantially reduced under water-saturated conditions by stiffening at low differential pressures.

Representative results for Cape Sorell quartzite

The low-frequency (0.01- to 1-Hz) shear modulus of the Cape Sorell quartzite is insensitive to pore-fluid saturation (Figure 3c). In contrast, at 1-MHz frequency, the shear modulus measured under argon-saturated conditions seems to be systematically slightly higher than for dry conditions (Figure 3c). Markedly more stiffening is observed for water-saturated conditions (Figure 3c). Such stiffening is most pronounced at low differential pressures (Figures 3a and 3b), and it diminishes gradually with increasing differential pressure.

Representative results for the cracked glass-bead specimen

Ultrasonic measurements on thermally cracked sintered glass-bead specimens also reveal a systematic increase of the shear modulus with increasing differential pressure (Figure 4). However, the range through which the modulus varies is substantially narrower than for the quartzite, as is the range of differential pressure across which the marked increase in modulus is observed. In contrast to the data for the Cape Sorell quartzite, a substantial increase of the shear

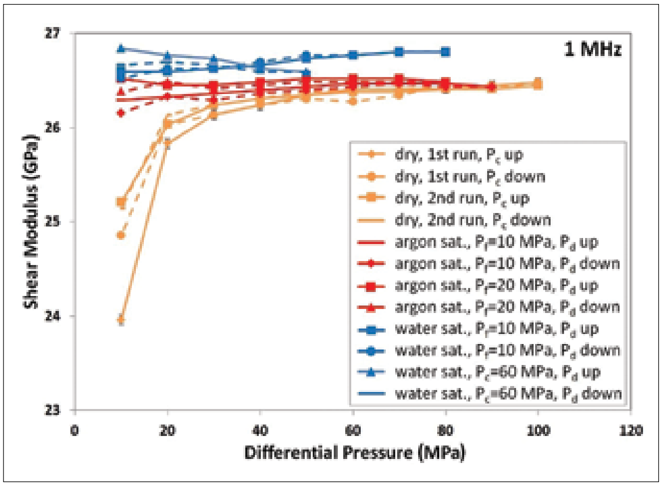

Figure 4. Shear modulus of the cracked glass-bead specimen measured under dry, argon-saturated, and water-saturated conditions at ultrasonic frequency. A systematic stiffening effect caused by pore-fluid saturation can be observed at this frequency. P_c, P_f, and P_d denote confining pressure, pore pressure, and differential pressure (confining pressure minus pore pressure), respectively. The labels *up* and *down* correspond, respectively, to data obtained during increasing and decreasing P_c or P_d.

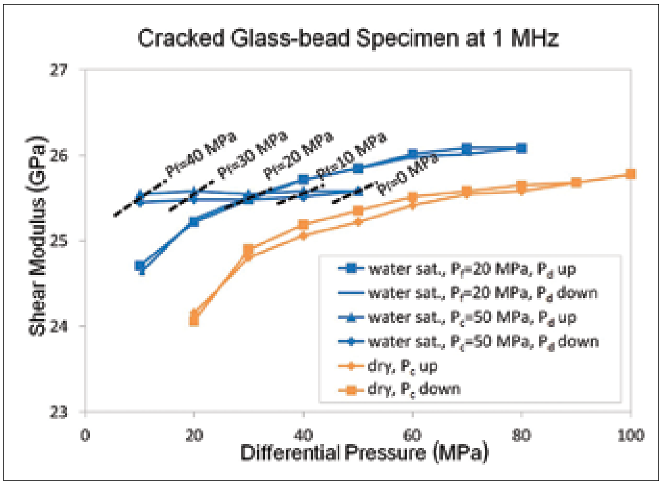

Figure 5. Shear modulus as a function of differential pressure for the cracked glass-bead specimen. Dry data are plotted as the baseline for the modulus increase caused by water saturation. There are two ways to systematically vary differential pressure and to achieve a common P_d value: vary the confining pressure while pore pressure is constant (isobar of P_f = 20 MPa) or vary the pore pressure and keep the confining pressure constant (P_c = 50 MPa). A consistent trend of higher overall shear modulus is observed when the saturating fluid is at a higher pore pressure but at the same differential pressure. This is highlighted by short dashed lines crossing observed data points.

modulus is found at megahertz frequency under argon-saturated and especially water-saturated conditions. Within the range of relatively low differential pressures, the shear modulus varies systematically with both differential pressure and pore-fluid pressure (Figure 5).

As various differential pressures are achieved by different combinations of confining and pore-fluid pressures, all measured data at the same pore-fluid pressure can be connected with pore-fluid isobars. From the measured isobar P_f = 20 MPa and other individual data acquired at pore-fluid pressures other than 20 MPa, we can observe a trend of systematic stiffening with increasing pore pressure at constant differential pressure. The dry megahertz data in Figure 5 define a baseline for evaluation of the influence of fluid saturation.

Discussion

The differential pressure needed to close a thin spheroidal crack that has an initial aspect ratio α is $P \sim E\alpha$ (Walsh, 1965), where E is Young's modulus of the solid. For the Cape Sorell quartzite ($E \approx 95$ GPa), the pressure dependence of the shear modulus is greatest for $P_d < 80$ MPa, consistent with the closure of thermal cracks of low aspect ratio $\alpha < 0.0008$. However, a substantial pressure sensitivity is maintained beyond 80 MPa, with shear modulus gradually approaching the Hashin-Shtrikman value of 44 GPa for uncracked quartzite, suggesting ongoing closure of cracks with aspect ratio $\alpha > 0.0008$ (Figure 3c).

For the glass-bead specimen, $E \approx 70$ GPa and $\alpha \approx 0.0007$, giving $P \approx 50$ MPa. Minimal pressure sensitivity of shear modulus for differential pressures $P_d > 50$ MPa (Figure 4) therefore indicates that the glass-bead specimen contains few cracks of aspect ratio greater than 0.0007 (nonclosable pores excepted).

The absence of observable stiffening of quartzite at low frequencies with either argon or water saturation (Figure 3c) agrees with the theoretical prediction that the dry modulus and low-frequency saturated-isobaric shear modulus should be equal, assuming no chemical interactions between the minerals and the fluid (Gassmann, 1951). The significant stiffening of the quartzite with water saturation at 1 MHz (Figure 3) suggests that the transition from the saturated-isobaric to the saturated-isolated fluid-flow regime is located between hertz and megahertz frequencies. This idea will be tested further below.

As described above, the shear modulus of the water-saturated glass-bead specimen depends on both differential pressure and pore-fluid pressure. The pore-pressure isobar and other measured data points (solid symbols and lines) highlight a systematic increase in shear modulus as the pressure of water pore fluid increases (Figure 4 and 5), the bulk modulus of which is 2.2 GPa at ambient pressure but increases with pressure.

Negligible change in water viscosity occurs over the pressure range measured. The results show that the effective shear modulus of a fluid-saturated rock is not a function solely of the differential pressure but also of the bulk modulus of pore fluid. The modest mismatch between the dry modulus and the water-saturated modulus at zero pore-fluid pressure can be attributed mostly to residual water trapped in the crack network (Figure 5).

David and Zimmerman (2012) propose a model to extract the crack-density parameter and the aspect-ratio distribution from the pressure dependence of dry elastic moduli, assuming that closable cracks and nonclosable pores can be represented as spheroids (a spheroid is an ellipsoid with two


www.polarcus.com/rightband
ARE YOU READY
FOR TRUE FIDELITY?
We are.
Through intelligent project design Polarcus can now deliver richer seismic images through precision optimization of acquisition and processing parameters for your specific geological objectives. The RIGHTBAND™ geophysical proposition has gained widespread industry acceptance for improving signal-to-noise over the whole desired frequency spectrum, with continuous recording instrumentation bringing deeper horizons into the picture.
Polarcus®

equal axes) that have an aspect ratio α. Such a model is applied here to the quartzite specimen. It should be noted that this method uses a pressure-dependent dry compressibility which can be extracted from joint measurements of compressional- and shear-wave velocities. Although we measured the compressional- and shear-wave velocities at ultrasonic frequencies, only shear-wave velocity data are presented in this article.

The value of the crack-density parameter, Γ, is first inferred at each pressure by inverting the deficits in the dry moduli relative to those of the uncracked material (Figure 6a), using the differential effective-medium scheme. The inverted values for the crack density closely fit an exponential decay function (Figure 6a), one advantage of which is to provide an extrapolated value of the "initial" crack density at zero pressure of 0.97 ± 0.08 and a characteristic pressure for crack closure of about 34 MPa. The large value of the crack density is consistent with the spectacular increase of dry shear modulus from 10 to 35 GPa, attributed to crack closure, whereas the characteristic crack-closure pressure is a somewhat more rigorous and accurate estimation compared with the foregoing estimate (50 MPa) via the theory of Walsh (1965).

David and Zimmerman (2012) explain in detail how to extract the crack aspect-ratio distribution from the pressure dependence of crack density by using an additional crack-closure equation to change variables from crack-closure pressure to crack aspect ratio. This process makes use of the exponential decay function of Figure 6a to obtain the distribution of crack aspect ratios.

Figure 6b shows the distribution of crack porosity contributed by cracks of different aspect ratio (at zero pressure). The results show that the crack porosity of the quartzite is dominated by cracks with aspect ratio distributed around a characteristic value of 0.001 and yield a plausible estimate for the total crack porosity of 0.35%.

The subsequent step in effective-medium modeling is to use the crack aspect-ratio distribution — inverted from dry data as described above — to predict argon-saturated and water-saturated velocities (Figure 6c). At a given differential pressure, the pore structure should be identical regardless of whether the rock is dry or saturated with fluid. By now considering fluid-saturated cracks, the equations for the differential scheme can therefore be used in the forward-modeling sense to yield the pressure-dependent saturated elastic moduli. By using such equations, it is assumed implicitly that fluid is trapped in each pore; hence, the predicted saturated shear modulus is representative of the saturated-isolated regime. By definition, such a regime occurs when the wave frequency is higher than the critical frequency for squirt flow, which is approximately equal to $K_0\alpha^3/\eta$, where K_0 is the solid's bulk modulus and η is the viscosity of the pore fluid (O'Connell and Budiansky, 1977).

Comparison of the model predictions and the ultrasonic velocity data for the argon-saturated Cape Sorell quartzite (Figure 6c) indicates that the model matches the data quite well. This means that the modest amount

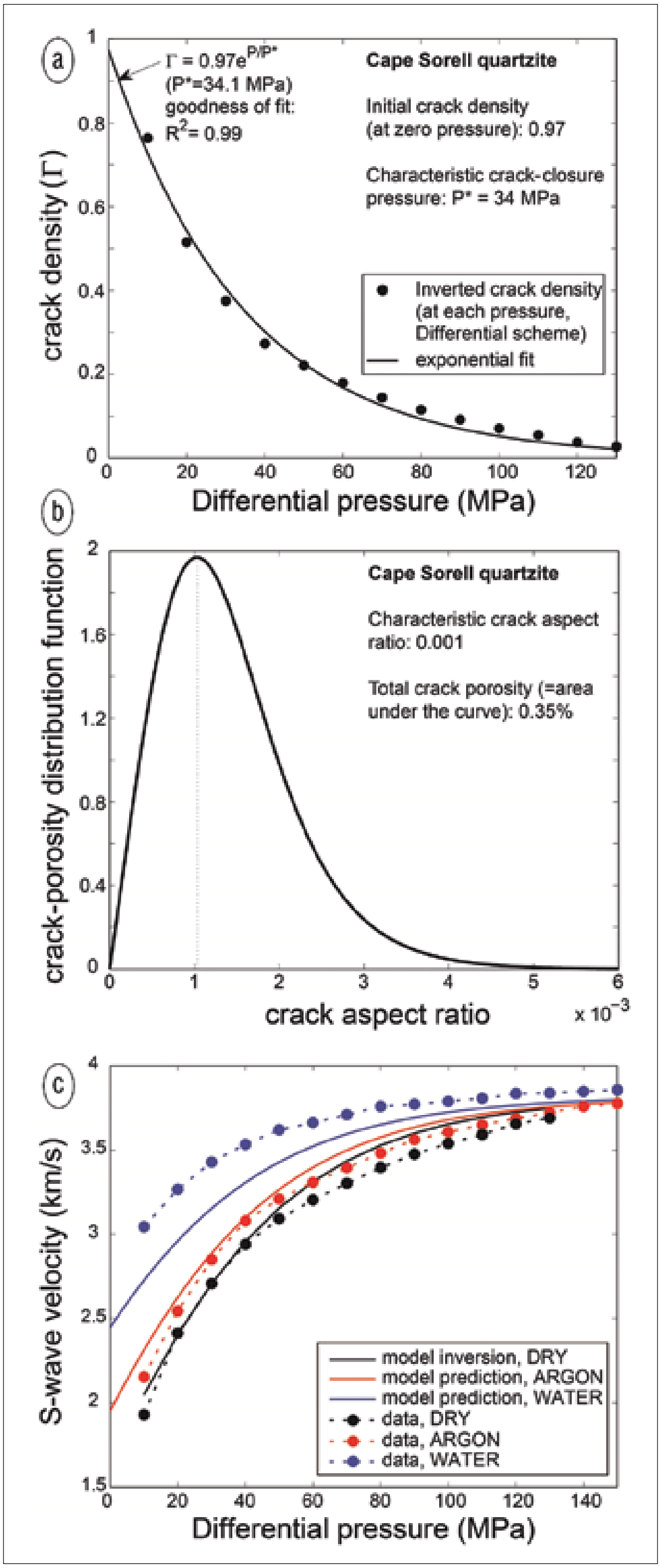

Figure 6. An interpretation of ultrasonic results on Cape Sorell quartzite, using the differential effective-medium scheme (David and Zimmerman, 2012): (a) crack density inferred at each pressure by inversion of the dry elastic modulus deficit relative to the uncracked material; (b) contribution to crack porosity as a function of crack aspect ratio; (c) model inversion of dry velocities and prediction of saturated velocities for both argon and water as saturants (lines) compared with ultrasonic data (symbols). Pore-fluid pressure for the predictions is set as 10 MPa.

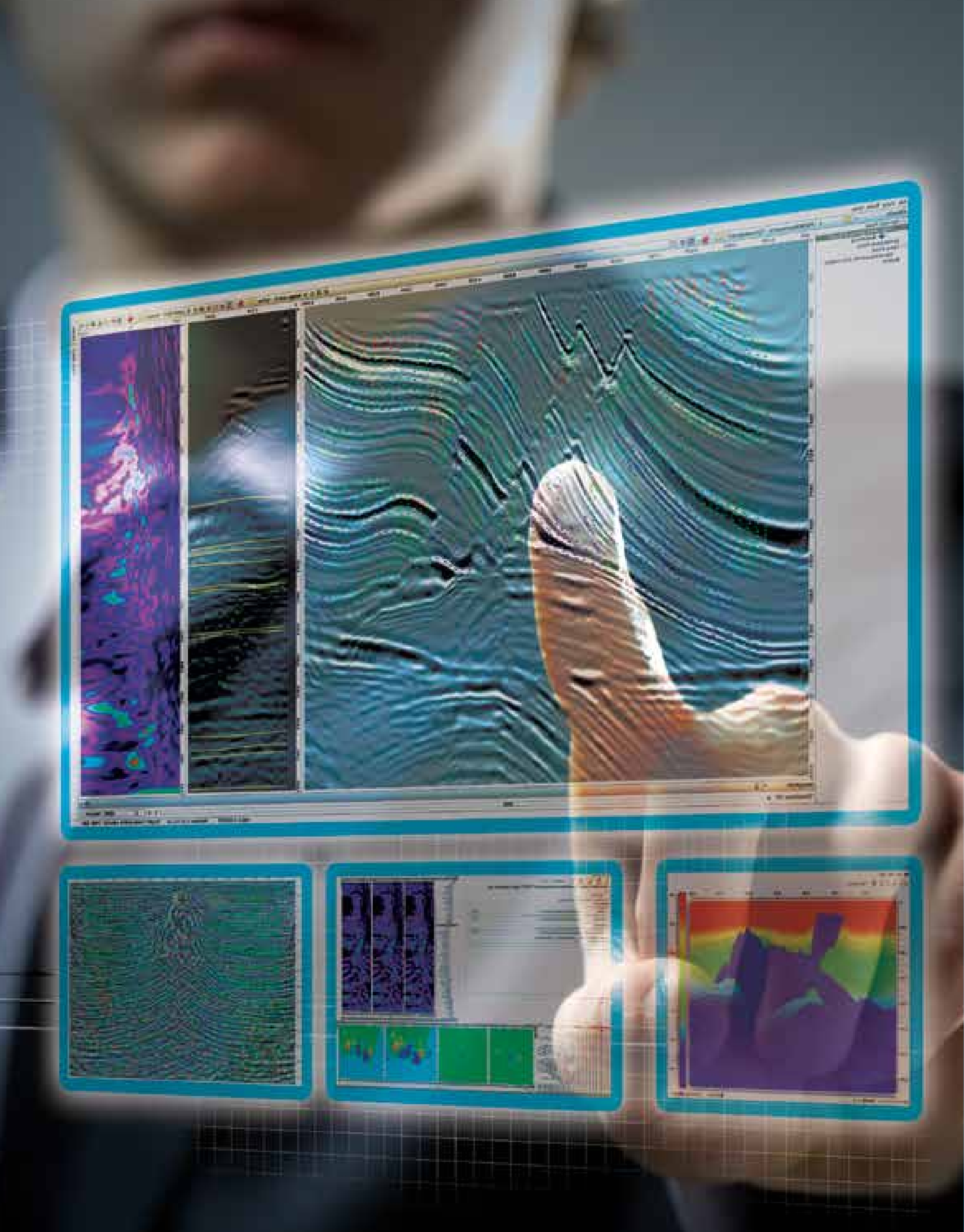

Z-TERRA

Z-Tomo should be an essential component of your workflow

Z-Terra Tomography Features

- Grid based tomography.
- VTI and TTI velocity updates.
- Single and multiple parameter residual velocity estimation.
- Wide azimuth backprojection updates.
- Selection of wide azimuth update geometry.
- Multiscale regularization tomography.
- Model preconditioning.
- Uses offset or angle gathers.
- Automatic residual velocity picking.
- Horizons and faults picking and visualization.
- Updates from topography.
- Automatically generated back-projection points.
- Use of horizons to constrain the velocity update.
- Layer freezing or global updates.
- Salt bodies insertion.
- Top and base salt horizon insertion.
- Salt flood model generation.
- Build complex overthrust and fault shadow velocity models.
- Global and local error visualization and QC.
- Residual error back-projection QC tools.
- Residual error smoothing along horizons.
- Ray coverage visualization and QC.
- Azimuth coverage visualization and QC.
- Checkpoint restart.
- Add and subtract nodes during runtime.
- Job monitoring.

Z-Terra has a wide range of velocity model building algorithms and workflows:

- Vertical and normal ray updates,
- Deregowski loop updates,
- Wide azimuth tomography using
  - offset gathers produced by Kirchhoff or Fast Beam Migration (FBM),
  - angle gathers produced by wave-equation migration,
  - angle gathers produced by Kirchhoff or FBM,
- Residual move-out gather-flattening and gather-fitting techniques,

The processing and visualization software is designed for rapid and accurate quality control and turnaround of the velocity iterations.

Revolutionary Tomography and Depth Velocity Model Building Starts Here

Z-Terra Inc.
17171 Park Row, Suite 247 • Houston, TX 77084
281.945.0000 www.z-terra.com
Contact us today at sales@z-terra.com.

of stiffening observed between dry and argon-saturated data makes quantitative sense for saturated-isolated conditions. Using O'Connell and Budiansky's (1977) equation, taking K_0 = 37 GPa (for quartz), α = 0.001 (cf. Figure 6b), and η = 0.03 mPa.s (for argon at 10 MPa), it is found that the characteristic squirt-flow frequency is approximately 1 MHz, marginally consistent with the conclusion concerning saturated-isolated conditions.

In the water-saturated case, it is certain that the quartzite lies in the saturated-isolated regime because water viscosity is higher than for argon by almost two orders of magnitude, giving the characteristic frequency of about 40 kHz. The fact that the model underestimates by about 30% to 40% the stiffening observed between dry and water-saturated tests suggests that some refinement might be needed for future application of the model to rocks other than sandstones, on which it was first demonstrated (David and Zimmerman, 2012). Nevertheless, the model provides a satisfying semiquantitative explanation for the velocities of the fluid-saturated quartzite, in addition to quantitative constraints on microstructural parameters.

Conclusions and prospects

Broadband measurements have clearly documented significant shear-modulus dispersion in the Cape Sorell quartzite from subhertz to megahertz frequencies with different saturants. The results on synthetic analogue at 1 MHz also demonstrate pore-pressure relaxations on different timescales by using saturants with different viscosities. The transition from saturated-isobaric to saturated-isolated fluid-flow regime clearly occurs between seismic and ultrasonic frequencies for the water-saturated Cape Sorell quartzite. Argon saturation shows a somewhat less spectacular but clear transition between fluid-flow regimes on the sintered glass-bead specimen, but such a conclusion is less certain for the Cape Sorell quartzite because of its higher crack aspect ratio.

Results from this broadband study reveal that seismic velocities obtained at ultrasonic frequencies can significantly overestimate the values relevant at seismic frequencies. In other words, ultrasonic measurements on rocks of low permeability might not be directly applicable to field data obtained by exploration seismic or sonic logging. Allowance must be made for the dispersion associated with local squirt flow on elastic wave speeds.

Future directions for this ongoing project include complementary ultrasonic measurements of compressional-wave speed and Young's modulus by flexural oscillation at subhertz frequencies on Cape Sorell quartzite and glass-bead materials. The resonant bar technique also will be used to provide access to intermediate "sonic" frequencies. The use of new synthetic samples of thermally cracked fully dense glass promises a cleaner separation of the roles of crack-pore and crack-crack local fluid flow. TLE

References

Adam, L., M. Batzle, and I. Brevik, 2006, Gassmann's fluid substitution and shear modulus variability in carbonates at laboratory seismic and ultrasonic frequencies: Geophysics, **71**, no. 6, F173–F183, http://dx.doi.org/10.1190/1.2358494.

Adam, L., M. Batzle, K. T. Lewallen, and K. van Wijk, 2009, Seismic wave attenuation in carbonates: Journal of Geophysical Research, **114**, B6, B06208, http://dx.doi.org/10.1029/2008JB005890.

Batzle, M. L., D.-H. Han, and R. Hofmann, 2006, Fluid mobility and frequency-dependent seismic velocity — Direct measurements: Geophysics, **71**, no. 1, N1–N9, http://dx.doi.org/10.1190/1.2159053.

Bouzidi, Y., and D. R. Schmitt, 2009, Measurement of the speed and attenuation of the Biot slow wave using a large ultrasonic transmitter: Journal of Geophysical Research, **114**, B8, B08201, http://dx.doi.org/10.1029/2008JB006018.

David, E. C., and R. W. Zimmerman, 2012, Pore structural model for elastic wave velocities in fluid-saturated sandstones: Journal of Geophysical Research, **117**, B7, B07210, http://dx.doi.org/10.1029/2012JB009195.

David, E. C., J. Fortin, A. Schubnel, Y. Guéguen, and R. W. Zimmerman, 2013, Laboratory measurements of low- and high-frequency elastic moduli in Fontainebleau Sandstone: Geophysics, **78**, no. 5, D369–D379, http://dx.doi.org/10.1190/geo2013-0070.1.

Gassmann, F., 1951, Über die Elastizität poroser Medien: Viertel-jahrsschrift der Naturforschen-den Gesellschaft in Zürich, **96**, 1–23.

Jackson, I., and M. S. Paterson, 1993, A high-pressure, high-temperature apparatus for studies of seismic-wave dispersion and attenuation: Pure and Applied Geophysics, **141**, nos. 2–4, 445–466, http://dx.doi.org/10.1007/BF00998339.

Mavko, G., and A. Nur, 1975, Melt squirt in the asthenosphere: Journal of Geophysical Research, **80**, no. 11, 1444–1448, http://dx.doi.org/10.1029/JB080i011p01444.

O'Connell, R. J., and B. Budiansky, 1977, Viscoelastic properties of fluid-saturated cracked solids: Journal of Geophysical Research, **82**, no. 36, 5719–5735, http://dx.doi.org/10.1029/JB082i036p05719.

Schijns, H., 2014, Experimental investigation of seismic velocity dispersion in cracked crystalline rock: Ph.D. thesis, University of Alberta.

Walsh, J. B., 1965, The effect of cracks on the compressibility of rocks: Journal of Geophysical Research, **70**, no. 2, 381–389, http://dx.doi.org/10.1029/JZ070i002p00381.

Acknowledgments: Financial support from the Australian Research Council (Grants DP08880453 and DP110101830), the Natural Sciences and Engineering Research Council of Canada (including the Alexander Graham Bell graduate scholarship and Michael Smith Foreign Study Supplement), and Alberta Innovates — Technology Futures is gratefully acknowledged. The editors and reviewers are thanked for helpful suggestions that significantly improved the manuscript.

Corresponding author: yang.li@anu.edu.au

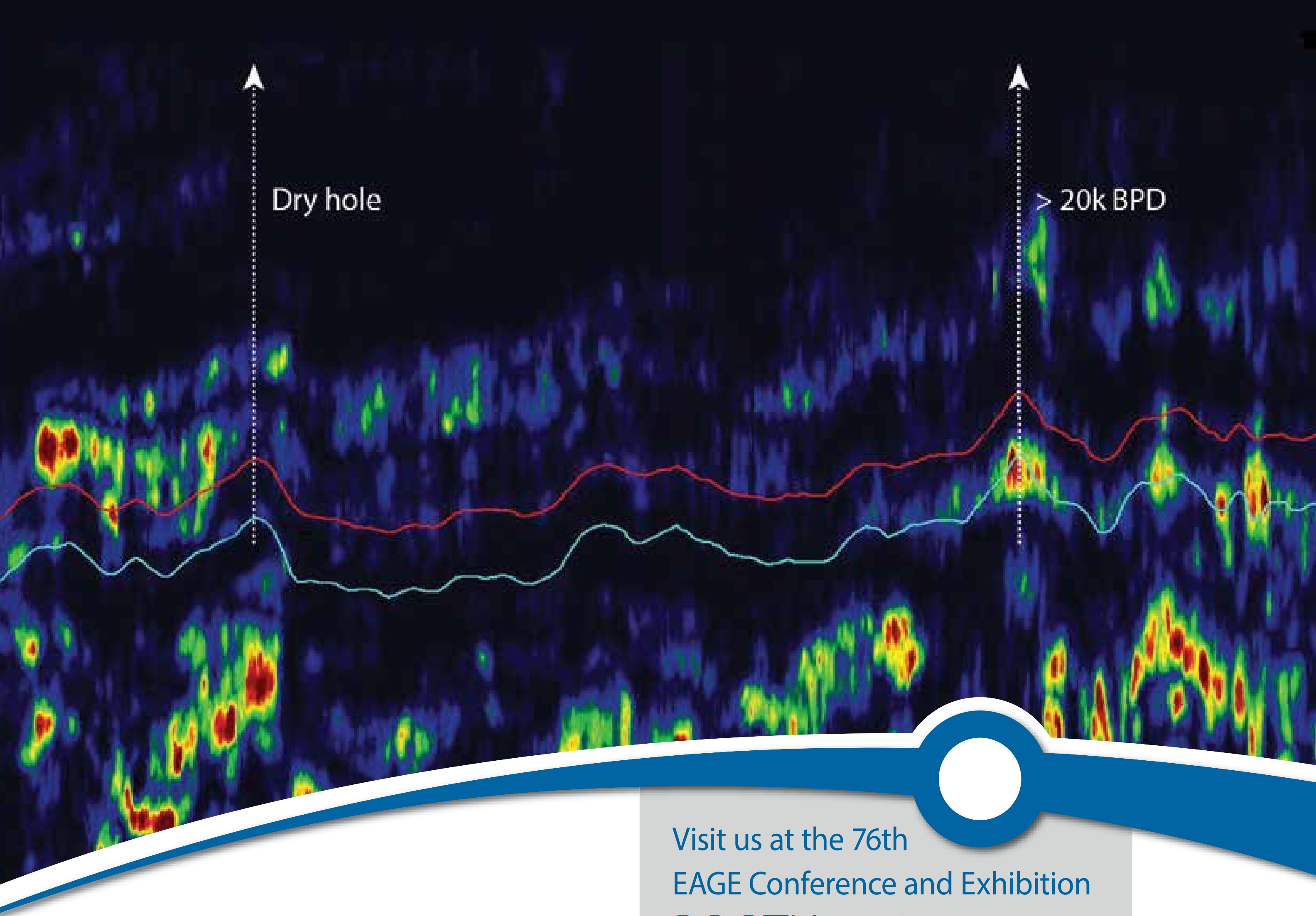
Dry hole
> 20k BPD